Journal of
Ceramic Science
and Technology

J. Ceram. Sci. Technol., **09** [3] 215-224 (2018)
DOI: 10.4416/JCST2018-00006
available online at: http://www.ceramic-science.com

Structure Features and Properties of Graphene/Al_2O_3 Composite

E. A. Klyatskina[2], A. Borrell[2], E. G. Grigoriev[1], A. G. Zholnin[1], M. D. Salvador[2], V. V. Stolyarov*[1, 3]

[1]National Research Nuclear University MEPhI (Moscow Engineering Physics Institute), Kashirskoye sh., 31, 115409 Moscow, Russia
[2]Instituto de Tecnología de Materiales, Universitat Politècnica de València, Camino de Vera s/n, 46022 Valencia, Spain
[3]Mechanical Engineering Research Institute of Russian Academy of Sciences 4, Maly Kharitonievsky line, 101990 Moscow, Russia
received January 24, 2018; received in revised form March 12, 2018; accepted March 19, 2018

Abstract

Since its discovery, graphene has attracted worldwide attention in the scientific community owing to its unique combination of properties. Thus, graphene is an ideal second phase to improve the structure and properties of metal, ceramic and polymer composite materials. This work presents a comparative study of two types of alumina-graphene composites fabricated with two sizes of δ-Al_2O_3 powders, nanometer and submicrometer, reinforced by graphene nanoplatelets (GNPs) and consolidated with the spark plasma sintering technique. The microstructure, mechanical and tribological properties of Al_2O_3-GNPs composites are influenced by the grain size of the ceramic matrix. Hardness values improve notably. The maximum value reached was 27.4 GPa for a composite fabricated with nanometric alumina powders, which is about 27 % higher than that of the Al_2O_3 monolithic material. Also, the methodology of powder mixing has a fundamental importance in obtaining materials with high-level properties.

Keywords: Graphene, nanocomposite, wear behavior, mechanical properties, SPS

I. Introduction

The technical interest in graphene application started with the publication of the work of Novoselov and Geim in 2005 [1]. This scientific team synthesized graphene from graphite by means of mechanical exfoliation. Since then, its various exceptional properties have allowed graphene to occupy a relevant space amongst other materials, and graphene has become one of the more plausible alternatives to carbon nanotubes in different applications [2–7].

Unlike a monolayer graphene, multilayer graphene nanosheets (MGN), graphene nanosheets (GNS) or graphene nanoplatelets (GNPs) are formed by several layers of graphene with a thickness up to 100 nm. GNPs have very distinct characteristics which, in the case of composite materials, make them very good nanofillers. Those characteristics include excellent mechanical properties, a large specific surface area and a geometry presenting a two-dimensional high aspect ratio [2–8].

This material features a unique combination of electrical, mechanical and thermal properties [8–10], and recently showed anti-cancer potential [11]. Several scientific works report the increment of fracture toughness and electrical conductivity up to 238 % and 1000 S/m, respectively [12, 13]. Therefore, graphene can be potentially used as a structural or functional material; moreover, there are electrical applications, for example, as a protective cover with microwave shielding ability [14]. It seems that the results depend on the kind of ceramic matrix. The use of nanograins of alumina could improve the final properties of these materials for multifunctional applications [15–17]. One of the clear advantages of graphene is derived from its surface area (e.g. a single layer of graphene shows 2630 m^2/g). Therefore, it can be very efficiently used to improve the properties of composites when used as a second phase, i.e. full coverage of a matrix could be obtained with only small amounts of graphene (less than 1 vol%) [18].

The spark plasma sintering technique (SPS) is currently used to obtain ceramic-graphene composites; this non-conventional technique preserves the integrity of graphene flakes from structural defects by minimizing the process time at high temperature. An additional application where graphene can excel is in the field of solid lubrication by protecting the coated surface [19, 20]. A second phase layer of graphene will induce a significant reduction of wear owing to a decrease in the friction forces produced between surfaces in contact on micrometric and nanometric scales [21–24]. However, looking in another direction, in order to explore graphene's full potential, tribological studies in the ranges of submicro- and nano-scales need to be completed, hitherto little work has been carried out and scope remains for the discovery of new applications.

Until now, the use of ceramic composites has mainly been developed within commercial applications, as wear-resis-

* Corresponding author: vlstol@mail.ru

tant coatings rather than structural body parts. However, to overcome typical drawbacks of ceramic composites such as brittleness under severe stress, ceramic composites have been reinforced with different carbon-based solutions like carbon nanofibers [19, 25], carbon nanotubes [3–6], or whiskers [26, 27]. The aim of this paper is to demonstrate the successful fabrication of alumina-graphene composites by employing alumina submicro- and nano-powders obtained by means of the oxidation of aluminum in an air plasma jet and using non-conventional techniques, such as spark plasma sintering. To the best of our knowledge, this is the first report on such novel composites with nano-alumina powders (particle sizes less than 50 nm). The effect of GNPs on the structure, morphology, tribological and mechanical properties of the composites sintered by means of SPS was studied and discussed.

II. Experimental

(1) Composite preparation

To obtain the advanced ceramic composites for the study, mixtures of alumina and graphene powders were used. For sample preparation, two particle sizes, nanometer and submicrometer, of δ-Al_2O_3 powders were obtained by means of the oxidation of aluminum in an air plasma jet and supplied by IMET RAS (Moscow, Russia), 45 ± 10 nm and 150 ± 15 nm, respectively were used.

Graphene nanoplatelet powders (GNPs), supplied by Graphene-tech (Zaragoza, Spain), were produced with the ultrasonic exfoliation method. The morphology of the different starting powders is shown in Fig. 1; Fig. 1c shows the multilayer scales of graphene with an average thickness of 3 nm (about 5 atomic layers) and 10 x 10 μm^2.

δ-Al_2O_3 powders and 0.5 wt% GNPs were dispersed in ethanol and then mixed in an ultrasonic bath under mechanical stirring. After that, the powder mixture was dried at 78 °C for 1 h on a heating plate to completely remove all the dispersant.

Finally, Al_2O_3-GNPs powders with nano and sub-micrometer particle sizes of alumina were sintered under vacuum with the spark plasma sintering technique (SPS, LABOX-625, SinterLand, Nagaoka City, Japan), where the powder was placed in a graphite die with an inner diameter of 15 mm. The sintering temperature was established at 1500 °C with a holding time of 10 min at the maximum temperature under an applied pressure of 50 MPa and a heating rate of 100 K/min. The optimum SPS conditions were chosen based on other studies carried out by the authors [20]. Afterwards, the sintered samples with 2 mm thickness were polished in order to complete measurement and analysis.

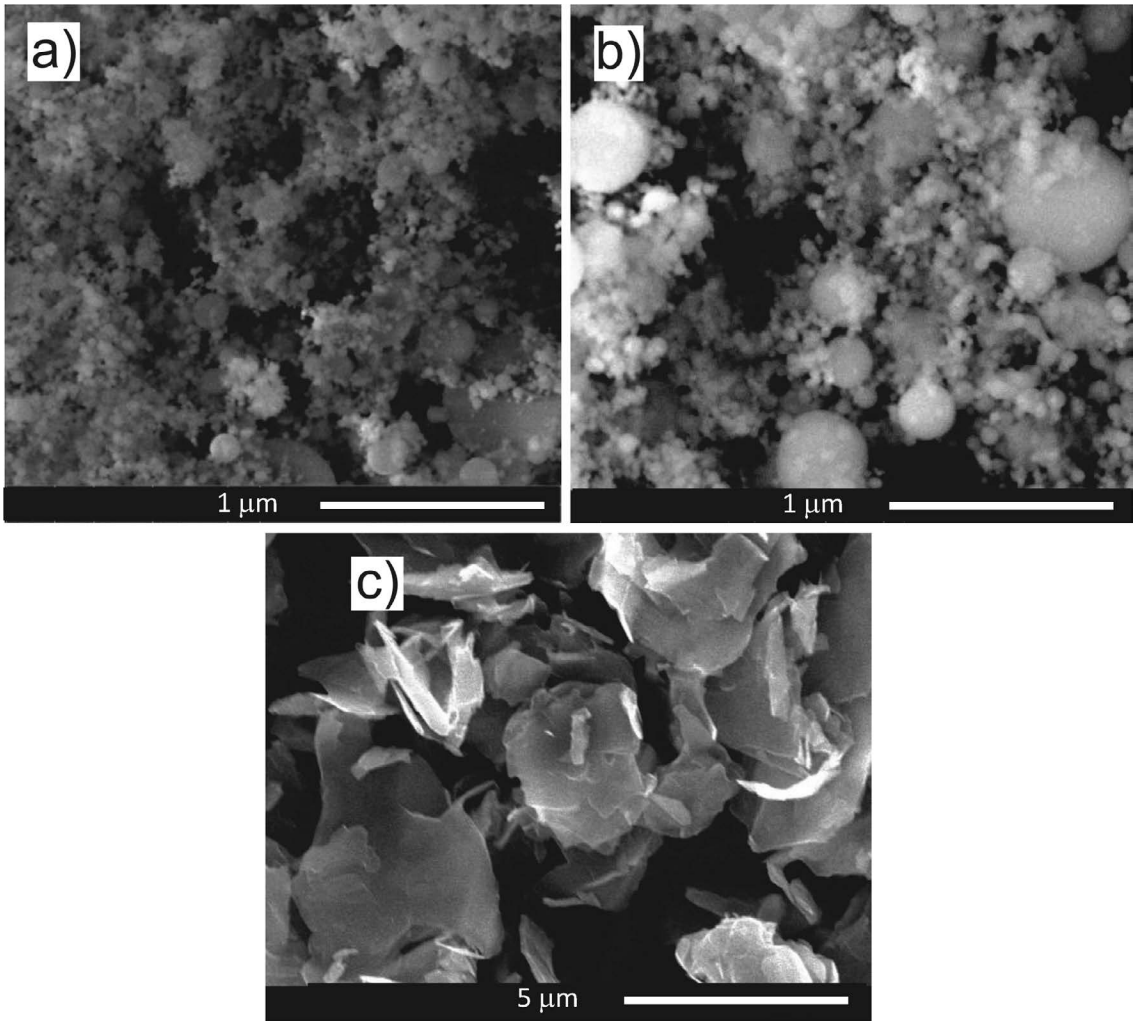

Fig. 1: FESEM images of the starting powders: (a) nanopowder δ-Al_2O_3, (b) sub-micrometer powder δ-Al_2O_3,and (c) graphene nanoplatelets (GNPs).

(2) Characterization

The bulk density of the samples was measured using the Archimedes' principle by immersing it into a water-based liquid (ASTM C373 – 88). The hardness values were measured along the diameter of the sample using the Vickers indentation method at a load of 20 N applied for 10 s (FM-800 Future-Tech, Kawasaki-City, Japan).

Nanomechanical properties such as hardness (H) and Young's modulus (E) of samples were obtained by means of the nanoindentation technique (Model G200, MTS Company, USA). To carry out very low depth indentations, a brand new Berkovich diamond tip was used with a radius of less than 20 nm as certified by the manufacturing company. In order to ensure the quality of the tip throughout the work, pre- and post-calibration procedures were performed for this indenter, ensuring the correct calibration of its function area and correct machine compliance. Before the nanoindenter testing, the samples were prepared with metallographic techniques. After the samples had been cut, their surface was lapped and then polished with diamond paste, with a final 0.25-μm polish. The nanomechanical properties of the Al_2O_3-GNPs composites were evaluated from the load-displacement nanoindentation data using the widely accepted Oliver and Pharr method [28]. An array of 25 indentations was performed at a constant 2000 nm depth on arbitrary zones of the sample, ensuring that a representative zone was analyzed. The location of each test was guided by an optical microscope.

The bending strength of composites was determined in the Quasar 50 machine by conducting bending tests to failure, using methods for brittle materials [29].

The morphology and microstructure of the fracture of the samples were characterized using a field emission scanning electron microscope (FESEM, ZEISS ULTRA 55, Oxford Instruments). A transmission electron microscope (TEM, JEOL JEM-1010, Japan) was employed to investigate the distribution of the GNPs in the alumina matrix.

The Raman spectra measurements were performed at room temperature using a Renishaw via spectrometer with $\lambda = 532$ nm laser. The optical microscopy was used to locate spot areas with 3 mm diameter for the following sample analysis. The incident power was carefully programmed to avoid laser-induced heating.

Sliding wear tests were conducted in dry conditions in a tribometer pin-on-disc (ball-on-disc configuration) manufactured by MICROTEST MT2/60/SCM/T (Madrid, Spain), according to the ASTM wear testing standard G99 – 03 [30]. As a counter material, a ball of α-Al_2O_3 produced by GMS Ball Co Ltd. with 2400 HV_{10} and 6 mm radius was used. The tests were performed under 40 N of contact load, sliding speed of 0.1 m/s, sliding distance of 2000 m and a wear track radius of 3 mm. Environmental conditions were controlled in all tests to a temperature of 23 ± 2 °C and 60 ± 2 % relative humidity. In order to obtain enough representative values, a series of three tests for each material was conducted. The sample surface was polished down to 1 μm and cleaned before and after the wear test. Wear track surfaces were examined with a scanning electron microscopy (SEM, JEOL SM-6300, Japan). The wear rate of each material was calculated according to Lancaster's wear equation [31], as follows:

$$k_v = \frac{V_{wear}}{F_N \times S} \left[mm^3\ N^{-1}\ m^{-1} \right] \quad (1)$$

where V_{wear} is the wear volume loss in mm^3, F_N is the applied normal contact load, expressed in N; and S is the sliding distance in m. The wear volume loss, V_{wear}, was determined based on the measured mass loss of the samples divided by the bulk density of each one. The wear mass loss was obtained by weighing the samples before and after the test.

III. Results and Discussion

(1) Structure and microstructure characterization

Raman spectroscopy was used to confirm the structural integrity of the graphene in the composites after the sintering process. Fig. 2 shows the Raman spectra of graphene-alumina composites sintered at 1500 °C. These spectra of the sintered composites (nano and sub-micro confirm that the graphene was only little or not damaged at all during the spark plasma sintering. In the Raman spectra, the position, width, height of the 2D band, as well as the J_D / J_G intensity ratio characterize the structural state of graphene itself [32]. There are three important bands for graphene characterization: the D-band (band of defects, at ~ 1351 cm^{-1}) corresponding to the breaks in the translational symmetry of the hexagonal lattice, the G-band (at ~ 1580 cm^{-1}) related to the C-C tangential vibrational mode of graphene-like surfaces and the 2D band which is sensitive to the aromatic C-structure at around 2695 cm^{-1} ascribed to the G + D combination mode induced by disorder of the D + D′ band. In the case of ceramic composites, the increase of I_D/I_G ratio corresponds to an increase in the amount of disorder enhancement and a decrease in the mean crystal size as reported in a previous work [33, 34].

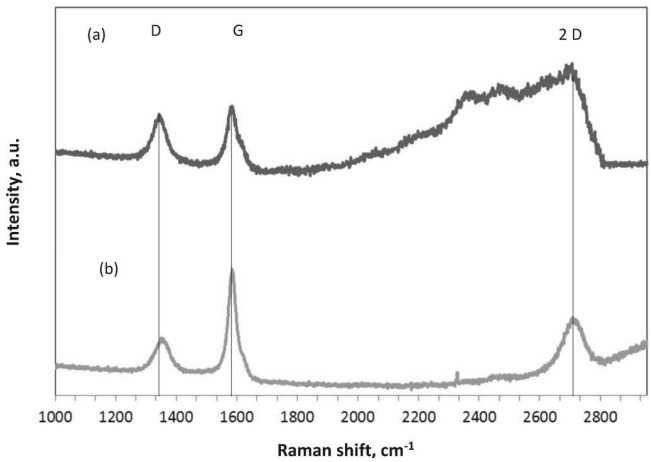

Fig. 2: Raman spectra of sintered samples by SPS: (a) Al_2O_3-GNPs nanocomposites and (b) Al_2O_3-GNPs sub-micrometer composites.

The 2D band of the nanocomposite consisting of two small peaks was numerically fitted by two Lorentzian line shapes as shown in Fig. 2a, where graphene has less than five layers and a doublet or multiple 2D band can be distinguished as revealed in previous results [35].

The increase in disordering in graphene, caused by a decrease in the grain size of the surrounding nano alumina matrix and, correspondingly, an increase in internal stresses, leads to an apparent broadening of the 2D peak. However, its position (2690 cm^{-1}) persists, which indicates the absence of graphene degradation. At the same time, it can be seen that the ratio of J_D/J_G decreases from 1 to 3, which may indicate partial amorphization of graphene [36].

In this study, it is shown that the allotropic form of GNPs is maintained in both types of composite obtained with SPS. For the nanocomposite, wider peaks are observed (Fig. 2a), the intensity ratio is greater than for sub-micro composites (Fig. 2b). Studies carried out in different sections showed the reproducibility of the results.

Sintered Al_2O_3-GNPs composites were fractured and their microstructures were examined. Fig. 3 shows the FE-SEM images of the fracture surfaces of the composites. It should be noted that after the SPS process the matrix grain size is much bigger in comparison with the particle size of the starting powders (Fig. 3a, b). The size of particles increased from nano and sub-micro size to several microns (Fig. 3c, d). It is important to note that a difference in the grain size between nano and sub-micro composites (see Fig. 3e, f) is observed. The grain growth is limited owing to the short cycle of sintering and fast heating of materials [37].

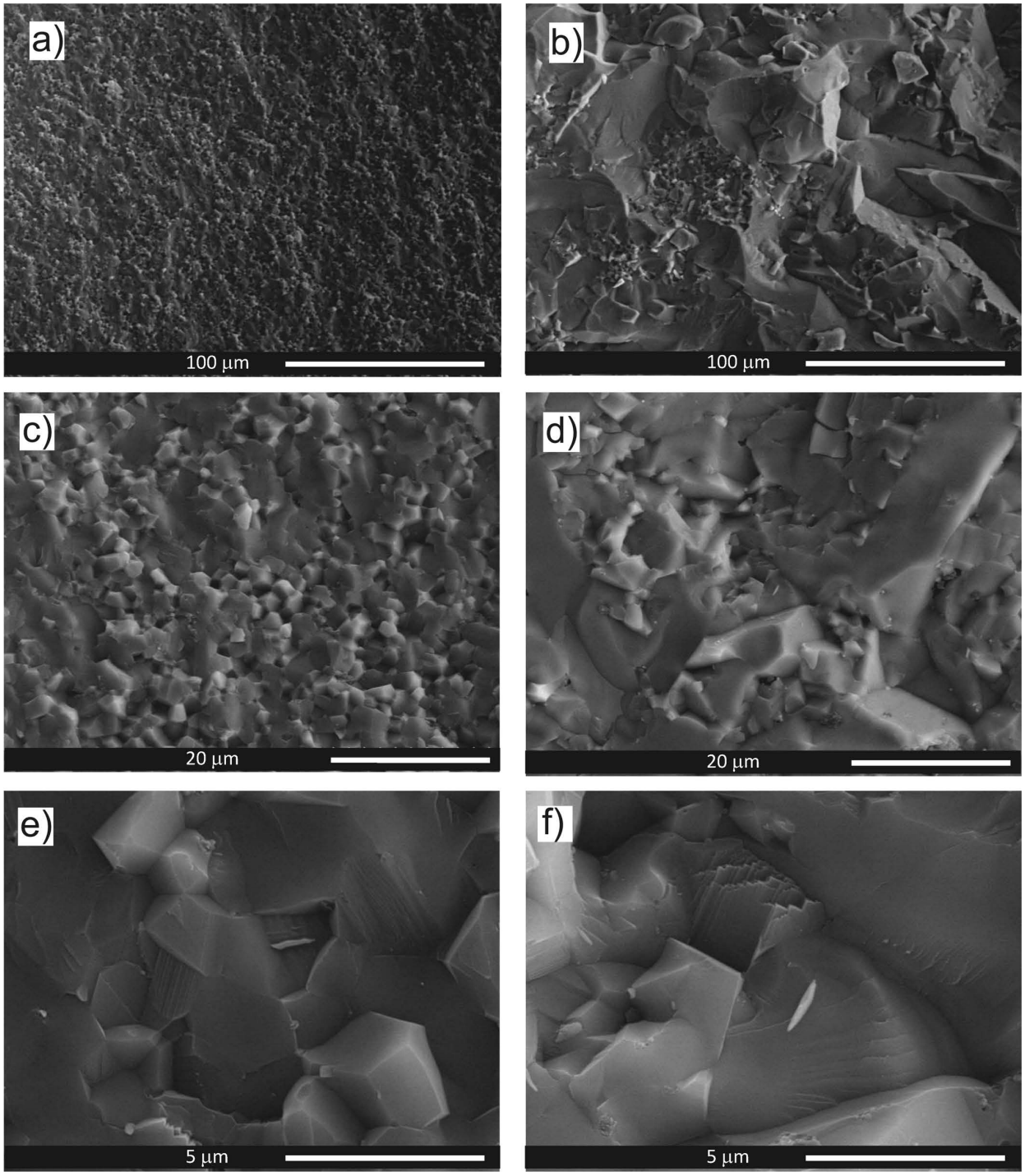

Fig. 3: FESEM images of fracture surfaces of: (a, c, e) Al_2O_3-GNPs nanocomposites and (b, d, f) sub-micrometer Al_2O_3-GNPs composites.

In Fig. 3e and 3f, it can be seen that the GNPs are placed inside the matrix grains. This allows the deduction that GNPs are distributed primarily at the boundary of the new grains formed during the SPS process. It is possible to conclude that the distribution of GNPs reduces the surface energy of the grain boundary, contributing to the stability of grain size or other properties of the material. The pulling-out length from alumina grain due to the interfacial friction between sheets and matrix is beneficial to improving the fracture toughness of the composite [38]. The addition of GNPs to the composite structure leads to a greater compression of the sample during sintering, which further leads to an increased contact level in the surface area between the powder particles, hence leading to the destruction of the sample following specific lattice failure patterns. The ductile fracture dominates under brittle mode and is determined by the mechanical properties of the powder particles. The recrystallization process during sintering does not affect the position in the matrix grain boundaries. The particle size and morphology of GNPs are not affected by the SPS since this process involves simultaneous synthesis and densification in a single step at comparatively low temperatures [39].

The microstructure of the composites was characterized by means of TEM. Fig. 4 shows TEM images of a sub-micrometric composite, indicating the high interfacial compatibility and wetting of GNPs to the matrix.

Fig. 4a shows that the GNPs are homogeneously distributed in the ceramic matrix. No intermediate phases could be detected at the interface, which shows that the GNPs and matrix are physically bonded together. TEM images show that the alumina phase has not changed and the electron diffraction data shown in Fig. 4b correspond to the alpha phase.

The location of the graphene within the composite structure is an important aspect. There are two kinds of GNP locations, at the grain boundaries and within the grains. On the one hand, it can be seen from Fig. 4a that inside alumina grains there are nano-particles presenting a scaly shape of a thickness of less than 1 nm. On the other hand, additional investigation in the dark field of the second phase, in contrast to the emission of carbon reflexes, showed the presence of graphene platelet shapes (Fig. 4b). Another important aspect is that during the SPS process the transition phase of alumina γ-Al_2O_3 to α-Al_2O_3 occurs along with grain growth caused by the migration of grain boundaries. As a result, graphene can be located inside and/or on the grain boundaries. The graphene nanoplatelets were found around small matrix grains and not around big ones. Therefore, the GNPs' presence inhibits alumina grain growth.

The mechanical properties and density of sintered samples are compiled in Table 1. The composites show density values above 98 % of theoretical density, which is less than for the pure alumina sample. As regards the mechanical properties, it can be seen that Al_2O_3-GNP composites exhibit higher mechanical properties than those of the alumina monolithic sample without graphene. Furthermore, the mechanical properties of all composites have been significantly improved. The hardness of the Al_2O_3-GNPs nanocomposites reaches a maximum value, which is about 25 – 30 % higher than that of the Al_2O_3 monolithic material and about 6 – 8 % higher than sub Al_2O_3-GNPs. The hardness values obtained for nanostructure composites are superior to those presented in previous studies of other authors with micrometric composites [40].

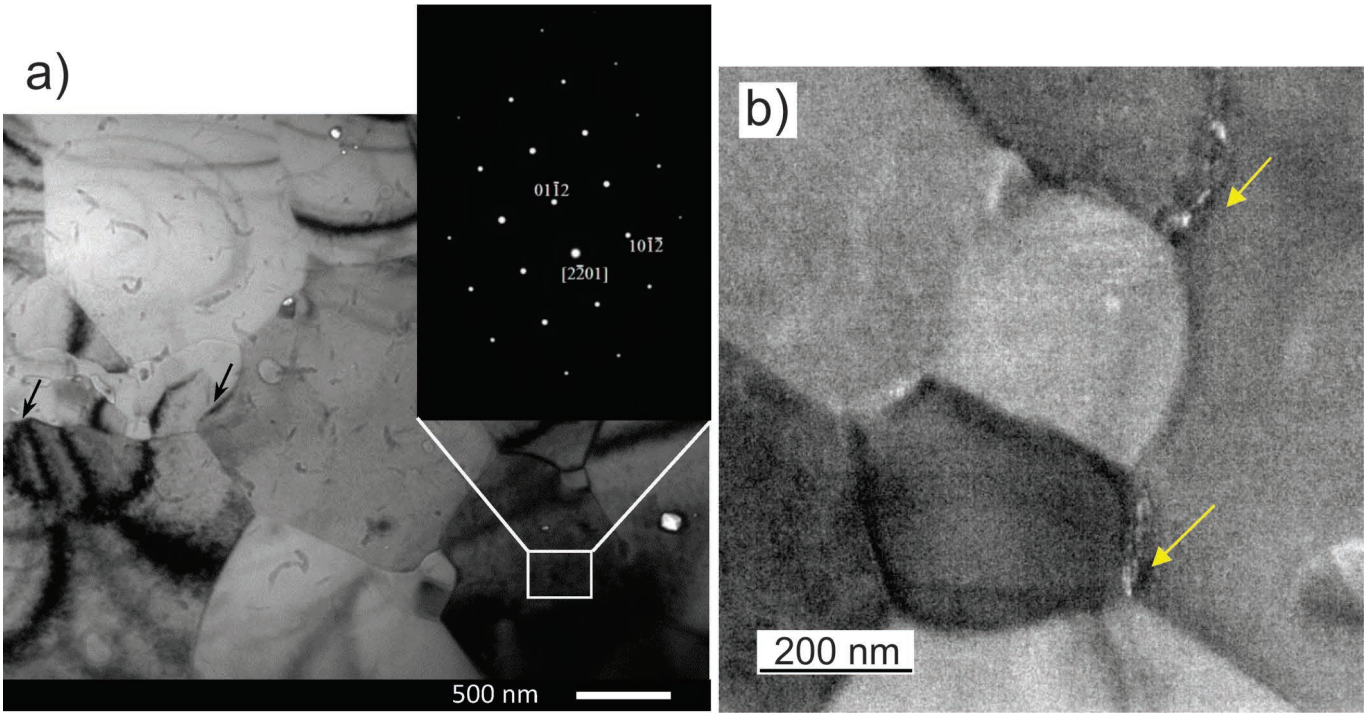

Fig. 4: TEM images of Al_2O_3-GNPs sub-micrometer composites: (a) bright field (BF) image with selected area diffraction pattern of Al_2O_3 grain and, (b) dark field (DF) image with bright zone indicating GNP locations (yellow arrows).

Table 1: Density and mechanical properties of sintered samples.

Samples	Density /g/cm^3	Relative density /%	Micro hardness, HV /GPa**)	Bending strength /MPa	Elastic modulus, E /GPa
Sub Al_2O_3*)	3.99 ±0.01	99.8±0.25	22±2	200±20	380±10
Sub Al_2O_3-GNPs	3.91±0.01	98.1±0.25	21.3±0.7	210±22	453±10
Nano Al_2O_3-GNPs	3.95±0.01	98.9±0.25	27.4±0.3	260±10	456±20

*) previous work [39]
**) previous work [41]

The evolution of the nanomechanical properties of Al_2O_3-GNPs composites – hardness (H) and Young's modulus (E), depending on penetration depth – can be seen in Fig. 5. The nanoindentation technique mainly developed by Oliver and Pharr has provided a reliable way to measure hardness and Young's modulus simultaneously by sensing the penetration depth of the indenter. The variations of the nanohardness values are small for all Al_2O_3-GNPs composites. N.S. Karthiselva *et al.* have mentioned in a previous work that the sub-micrometric sintered alumina samples without graphene achieved higher results for density, microhardness and strength than the nanometric alumina samples [40].

The arithmetic average of H and E values was calculated between 300 and 1000 nm depth ranges adopted to avoid crack gross effect in the deeper penetration. It is possible to observe that the H curve has a small tendency to decrease from 800 nm of depth penetration in the nanocomposites. This could be due to the brittle behavior of these materials or the effect of high grain boundary density. The average values are H = 25 GPa and E = 457 GPa for sub-micrometric composites, and H= 26 GPa and E = 453 GPa for nanometric composites; in agreement with the data reported by other authors [41, 42]. In general, nano- and sub-micrometer materials exhibited similar mechanical values.

Table 2 shows wear and friction coefficient values for all tested materials. As can be seen, the sub-micrometric material showed the worst sliding wear resistance in comparison with the nanometric material. Indeed, the nanometric material showed an increment of 1.8 times in wear resistance compared with the sub-micrometric materials. The wear rate of the ceramics is related to the grain size because the critical strain for grain boundary cracking decreases with increasing grain size and, therefore, the number of pull-outs is reduced [43]. Therefore, the improvement in wear resistance of the nanometric material should be attributed to the nanometric scale of grain size, which improves its physical and chemical and also mechanical properties.

FESEM micrographs of the wear tracks of both composites after the sliding wear tests are shown in Fig. 6. The first observation clearly shows the influence of an improved microstructure as in the nanometric materials, with regard to wear mechanisms. Thus, the sub-micrometric composites in Fig. 6a present the worst wear pattern damage of the two materials.

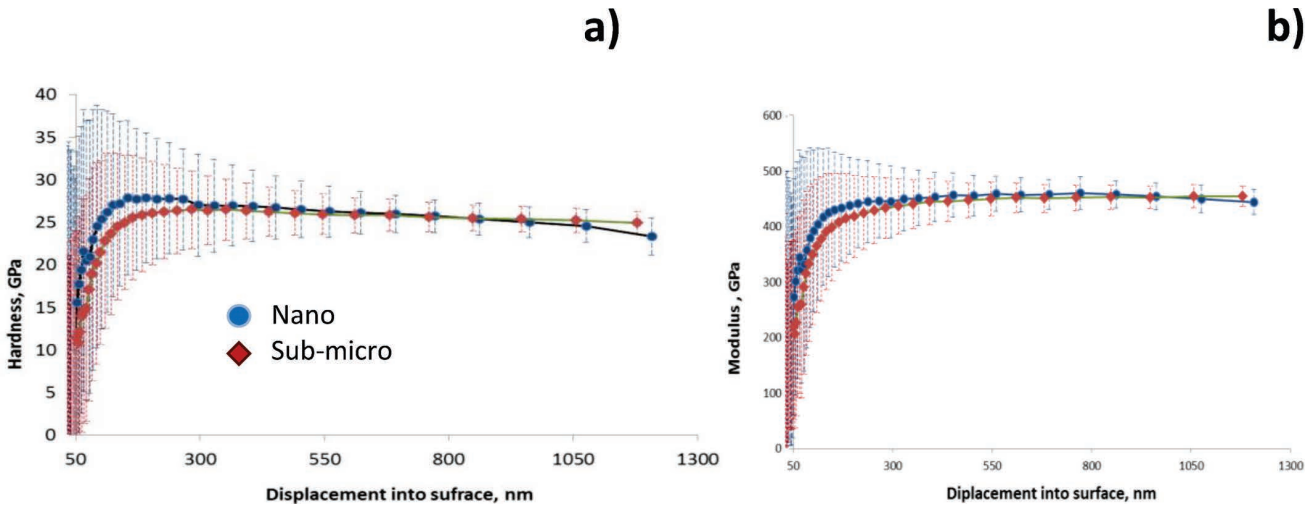

Fig. 5: Evolution in nanomechanical properties of alumina-graphene composites as a function of indentation depth and alumina grain size: (a) hardness and (b) Young's modulus.

Table 2: Wear and friction coefficient values of evaluated materials.

Samples	Vw (10^{-3} mm^3)	Kv (10^{-6} mm^3/N·m)	Friction coefficient
Sub Al_2O_3-GNPs	6.38±0.11	7.97±0.05	0.61±0.05
Nano Al_2O_3-GNPs	3.54±0.10	4.42±0.05	0.53±0.05

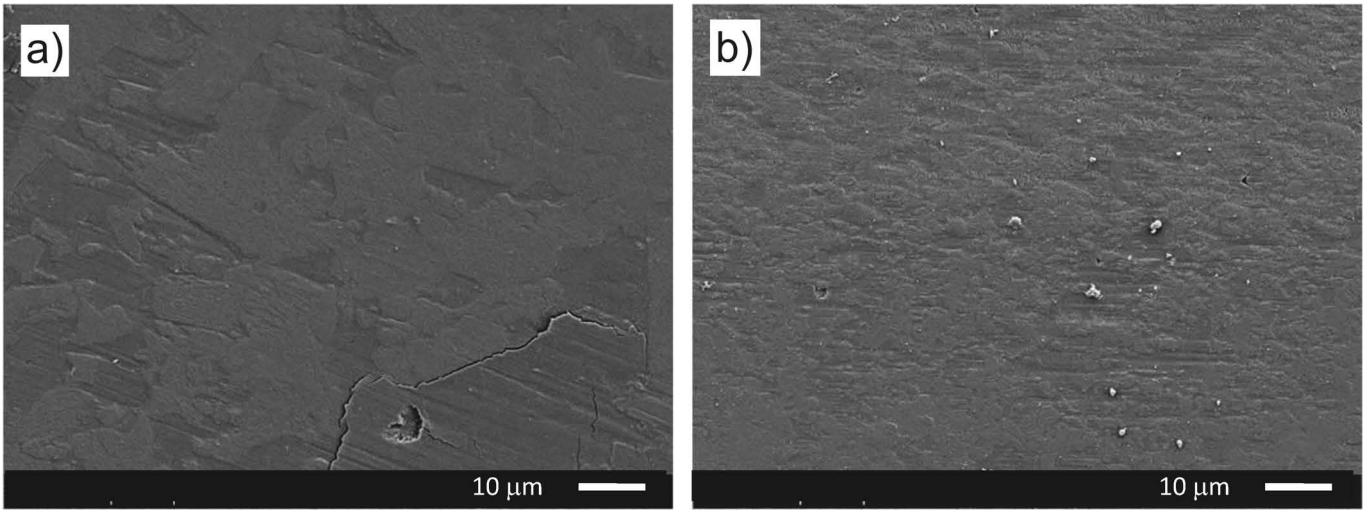

Fig. 6: Micrographs of the wear track in the surface of: (a) Al_2O_3-GNPs sub-micrometric composites and (b) Al_2O_3-GNPs nanocomposites.

Different wear process stages are shown in both composites: initial wear stage of the nanometric samples and progressive wear stage of the sub-micrometric samples [43]. In both composites the coexistence of various wear mechanisms is observed: polishing, abrasion, pull-out of grains, tribolayer formation and brittle fracture.

The increasing resistance of the sub-micrometric composites is proved by the existence of grooving in the sliding direction due to abrasion, perpendicular cracks towards the sliding direction related to brittle fracture, and holes caused by grain removal, and tribolayer formation in some areas. Material removal occurs during the cracking of big grains and pulling-out of individual grains, which causes holes in the contact surface. These holes in the contact surface are filled with wear debris platelets generated by the abrasive mechanism, which contribute to the creation of a tribolayer in the contact surface.

The tribolayer is a new surface with different mechanical characteristics compared to the original surface. This tribolayer contributes to the appearance of brittle fracture, crack formation and the deterioration of the contact surface. Nanocomposite shows a generation of wear debris (see bright spots in Fig. 6b), which still remains in the sliding surface and can act as a third body in the contact. Production of wear debris should be related to the pull-out of grains in the surface of the nanometric material and to the wear of the counterpart (Al_2O_3 ball). Also, we can observe an adhered material in the contact surface and plowing in the sliding direction, which causes abrasion. While the reduction in the grain size does not prevent pull-out of individual grains from the contact surface, it does prevent the removal of big sections of material.

IV. Conclusions

1. Novel Al_2O_3-GNPs composites were densified (~ 99 %) with non-conventional spark plasma sintering technology at 1500 °C and the wet ultrasonic mixing method and nanometric alumina powder.
2. Raman spectroscopy confirmed the high stability and uniform distribution of GPS in nano- and sub-micro composites.
3. The mechanical and tribological properties of Al_2O_3 matrix composites with additions of GNPs (such as wear resistance, friction coefficient, bending strength, hardness) were improved. The methodology of powder mixing had a fundamental importance in obtaining these nanocomposites with high-level mechanical and functional properties.
4. TEM images confirm that the occurrence of graphene nanoplatelets around small matrix grain contributes to a decrease in grain growth.
5. The sub-micrometric material showed the worst sliding wear resistance in comparison with the nanostructured material. Therefore, the improvement in the wear resistance of the nanocomposites should be attributed to the nature of nanometric scale grain size, which improves its physical and chemical as well as its mechanical properties.

The results of this work indicate the high potential of GNPs and SPS technology to suit various engineering applications of ceramic composites.

Acknowledgements

This work has been supported by the Competitiveness Program National Research Nuclear University MEPhI (Moscow Engineering Physics Institute), Russian Ministry of Education and Science No. 02. A 03.21.0005; the Russian Science Foundation N°16 – 19 – 10213; the Spanish Ministry of Economy and Competitiveness project MAT2015 – 67586-C3-R. E. Klyatskina acknowledges the Valencian Government for her Post-Doc. Contract APOSTD/2014/046 and A. Borrell acknowledges the Spanish Ministry of Economy and Competitiveness for her contract RYC2016 – 20915. The authors would like to thank Dr. Conrado R.M. Afonso, Universidad Federal de São Carlos, Brazil and Structure Investigation Department of Institute of Organic Chemistry, RAS for EF-TEM and SEM investigations.

References

1 Novoselov, K.S., Geim, A.K., Morozov, S.V. *et al.*: Two-dimensional gas of massless dirac fermions in graphene, *Nature*, **438**, 197 – 200, (2005).

2 Schwierz, F.: The rise and rise of graphene, *Nature Nanotech.*, **5**, 755, (2010).

3 Cheng, Z.G., Zhou, Q.Y., Wang, C.X. *et al.*: Toward intrinsic graphene surfaces: a systematic study on thermal annealing and wet-chemical treatment of SiO_2-supported graphene devices, *Nano Lett.*, **11**, 767 – 771, (2011).

4 Seema, H., Kemp, K.C., Chandra, V., Kim, K.S.: Graphene-SnO_2 composites for highly efficient photocatalytic degradation of methylene blue under sunlight, *Nanotechnology*, **7**, 23, (2012) 355705. doi: 10.1088/0957 – 4484/23/35/355705.

5 Nieto, A., Bisht, A., Lahiri, D., Zhang, C., Agarwal, A.: Graphene reinforced metal and ceramic matrix composites: a review, *J. Inter. Mat. Rev.*, **62**, 241 – 302, (2017).

6 Markandan, K., Chin, J.K., Tan, M.T.T.: Recent progress in graphene based ceramic composites: A review, *J. Mater. Res.*, **32**, 84 – 106, (2017).

7 Stankovich, S. *et al.*: Graphene-based composite materials, *Nature*, **442**, 282 – 284, (2006).

8 Soldano, C., Mahmood, A., Dujardin, E.: Production, properties, and potential of graphene, *Carbon*, **482**, 127 – 215 (2010).

9 Balandin, A.A., Ghosh, S., Bao, W. *et al.*: Superior thermal conductivity of single-layer graphene, *Nano. Lett.*, **3**, 902 – 907, (2008).

10 Frank, I.W., Tanenbaum, D.M., Vander Zande, A.M., McEuen, P.L.: Mechanical properties of suspended graphene sheet, *J. Vac. Sci. Technol.*, **6**, 2558 – 2561, (2007).

11 Paddock, C.: Graphene shows anticancer potential, *Medical News Today*, (2015).

12 Walker, L.S., Moratto, V.R., Raifee, M.A., Koratkar, N., Korall, E.L.: Toughening in graphene ceramic composite, *ASC Nano*., **5**, 3182 – 3190, (2011).

13 Centeno, A., Rocha, V.G., Alonso, B., Fernández, A. *et al.*: Graphene for tough and electroconductive alumina ceramics, *J. Eur. Ceram. Soc.*, **33**, 3201 – 3210, (2013).

14 Miranzo, P., Belmonte, M., Osendi, M.I.: From bulk to cellular structures: A review on ceramic/graphene filler composites, *J. Eur. Ceram. Soc.*, **37**, 3649 – 3672, (2017).

15 Kostecki, M., Grybczuk, M., Klimczyk, P. *et al.*: Structural and mechanical aspects of multilayer graphene addition in alumina matrix composites-validation of computer simulation model, *J. Eur. Ceram. Soc.*, **36**, 4171 – 4179, (2016).

16 Tubío, C.R., Rama, A., Gómez, M. *et al.*: 3D-printed graphene-Al_2O_3 composites with complex mesoscale architecture, *Ceram. Int.*, **44**, 5760 – 5767, (2018).

17 Porwal, H., Saggar, R., Tatark, P. *et al.*: Effect of lateral size of graphene nano-sheets on the mechanical properties and machinability of alumina nano-composite, *Ceram. Int.*, **42**, 7533 – 7542, (2016).

18 Niihara, K.: New design concept of structural ceramics-ceramic nanocomposites, *J. Ceram. Soc. Jpn.*, **99**, 974 – 982, (1991).

19 Borrell, A., Torrecillas, R., Rocha, V.G., Fernández, A.: Alumina-carbon nanofibers nanocomposites obtained by spark plasma sintering for proton exchange membrane, *Fuel Cells*, **12**, 599 – 605, (2012).

20 Zholnin, A.G., Kovaleva, I.V., Yurlova, M.C., Ilina A.M. *et al.*: Uniaxial magnetic pulsed compaction of α-Al_2O_3 nano powders followed by conventional and spark-plasma sintering, *Phys. Chem. Mat. Procs.*, **2**, 73 – 79, (2015).

21 Kim, H.J. *et al.*: Unoxidized Graphene/Alumina Nanocomposite: Fracture- and wear-resistance effects of graphene on alumina matrix, *Sci. Rep.*, **4**, 5176, (2014).

22 Borrell, A., Torrecillas, R., Rocha, V.G., Fernández, A. *et al.*: Effect of CNFs content on the tribological behaviour of spark plasma sintering ceramic-CNFs composites, *Wear*, **274**, 94 – 99, (2012).

23 Morgiel, J., Klimczyk, P., Major L. *et al.*: TEM investigations of wear mechanism of Al_2O_3 and Si_3N_4 compacts with GLPs additions, *Ceram Int.*, **43**, 8334 – 8342, (2017).

24 Cano-Crespo, R., Moshtaghioun, B.M., Gómez-García, D. *et al.*: High-temperature creep of carbon nanofiber-reinforced and graphene oxide-reinforced alumina composites sintered by spark plasma sintering, *Ceram. Int.*, **43**, 7136 – 7141, (2017).

25 Borrell, A., Torrecillas, R., Rocha, V.G., Fernández, A. *et al.*: Improvement of CNFs/ZrO_2 composites properties with a zirconia nanocoating on carbon nanofibers by sol-gel method, *J. Am. Ceram. Soc.*, **94**, 2048 – 2052, (2011).

26 Zhang, X., Xu, L., Du, S., Han, W., Han, J.: Crack-healing behavior of zirconium diboride composite reinforced with silicon carbide whiskers, *Scripta Mater.*, **59**, 1222 – 1225, (2008).

27 Zhao, J. *et al.*: Mechanical behavior of alumina-silicon carbide nanocomposites, *J. Am. Ceram. Soc.*, **76**, 503 – 510, (1993).

28 Oliver, W.C. Pharr, G.M.: An improved technique for determining hardness and elastic-modulus using load and displacement sensing indentation experiments, *J. Mater. Res.*, **7**, 1564 – 1583, (1992).

29 Tumanov, A.T.: Methods of testing, monitoring and investigation of engineering materials T. II. Methods of study of the mechanical properties of metals, *M.: Mashinostroenie*, 320, (1974).

30 ASTM International: (2003) ASTM G99 – 03: Standard test method for wear testing with a pin-on-disc apparatus. ASTM annual book of standards. ASTM International: West Conshohocken

31 Lancaster, K.: The influence of substrate hardness on the formation and endurance of molybdenum disulphide films, *Wear*, **10**, 103 – 107, (1967).

32 Childres, I., Jauregui, L.A., Park, W. *et al.*: New Developments in Photon and Materials Research: Chapter 19: Raman spectroscopy of graphene and related materials, (2013) ISBN: 978-1-62618-384-1

33 Xia, H., Zhang, X., Shi, Z., Zhao, C. *et al.*: Mechanical and thermal properties of reduced graphene oxide reinforced aluminum nitride ceramic composites, *Mater. Sci. Eng.*, **639**, 29 – 36, (2015).

34 Inam, F., Vo, T., Bhat, B.R.: Structural stability studies of graphene in sintered ceramic nanocomposites, *Ceram. Int.*, **40**, 16227 – 16233, (2014).

35 Benavente, R., Pruna, A., Borrell, A., Salvador M.D. *et al.*: Fast route to obtain Al_2O_3-based nanocomposites employing graphene oxide: Synthesis and sintering, *Mater. Res. Bull.*, **64**, 245 – 251, (2015).

36 Lucchese, M.M., Stavale, F., Ferreira, E.H.M. *et al.*: Quantifying ion-induced defects and raman relaxation length in graphene, *Carbon*, **48**, 1592 – 1597, (2010).

37 Kovaleva, I., Zholnin, A., Grigoryev, E., Olevsky, E.: Magnetic pulse compaction and subsequent spark plasma sintering of nanostructured alumina, Proc. from Congress Machin. Technol. Mat. Varna, Bulgaria, (2015).

38 Wang, K. *et al.*: Preparation of graphene nanosheet/alumina composites by spark plasma sintering, *Mater. Res. Bull.*, **46**, 315 – 318, (2011).

39 Zholnin, A.G. Kovaleva, I.V., Yu, V., Rytenko, Pahilo-Daryal, I.O. *et al.*: Effect of particle size of alumina powder on spark-plasma sintering, *Phys. Chem. Mat. Procs.*, **1**, 53 – 63, (2016).

[40] Karthiselva, N.S., Bakshi, S.R.: Carbon nanotube and *in-situ* titanium carbide reinforced titanium diboride matrix composites synthesized by reactive spark plasma sintering, *Mater. Sci. Eng.*, **663**, 38 – 48, (2016).

[41] Stolyarov, V.V., Misochenko A.A. *et al.*: Structure and properties of Al_2O_3/Graphene nanocomposite processed by spark plasma sintering, *IOP Conf. Series: Mater. Sci. Eng.*, 218, (2017).

[42] Gutierrez-Gonzalez, C.F. Smirnov, A., Centeno, A. *et al.*: Wear behavior of graphene/alumina composite, *Ceram. Int.*, **41**, 7434 – 7438, (2015).

[43] Denape, J.: Wear Debris Action in Sliding Friction of Ceramics. *Tribology Series* **21** (1992) 453 – 462